Hindawi Publishing Corporation
Journal of Nanomaterials
Volume 2015, Article ID 213128, 12 pages
http://dx.doi.org/10.1155/2015/213128

Research Article

Oxidation and Corrosion Behavior of Nanolaminated MAX-Phase Ti_2AlC Film Synthesized by High-Power Impulse Magnetron Sputtering and Annealing

Jianjian Fu,[1] Teng Fei Zhang,[2,3] Qixun Xia,[1] Sung-Hwan Lim,[4] Zhixin Wan,[2,3] Taeg-Woo Lee,[4] and Kwang Ho Kim[1,3]

[1]*School of Materials Science and Engineering, Pusan National University, Busan 609-735, Republic of Korea*
[2]*Department of Applied Hybrid Materials, School of Convergence Science, Pusan National University, Busan 609-735, Republic of Korea*
[3]*Global Frontier Center for Hybrid Interface Materials, Pusan National University, Busan 609-735, Republic of Korea*
[4]*Department of Advanced Materials Science and Engineering, Kangwon National University, Chuncheon 24341, Republic of Korea*

Correspondence should be addressed to Kwang Ho Kim; kwhokim@pusan.ac.kr

Received 11 September 2015; Revised 19 November 2015; Accepted 24 November 2015

Academic Editor: Je M. Yun

Nanolaminated MAX-phase Ti_2AlC thin films were synthesized by high-power impulse magnetron sputtering (HiPIMS) from a MAX-phase Ti_2AlC target. The amorphous matrix Ti-Al-C films were deposited at room temperature, while the MAX-phase Ti_2AlC films were obtained through annealing process of the as-deposited amorphous matrix films. The microstructure, oxidation resistance, and corrosion behavior of these two films were comparatively investigated. The results indicated that the MAX-phase Ti_2AlC films had superior antioxidation and anticorrosion properties than the amorphous matrix Ti-Al-C films, which is attributed to the rapid formation of dense Al_2O_3 layer on the top of MAX-phase Ti_2AlC films because of the rapid diffusion of Al atoms in the typical nanolaminated structure of MAX phase.

1. Introduction

$M_{n+1}AX_n$ phases (MAX phases), one kind of nanolaminated carbides or nitrides (M: early transition metal, A: an element of group IIIA or IVA, and X: C and/or N) [1–4], have gained significant attention on the theoretical and experimental studies since they were discovered in 1960s [5, 6]. They possess excellent and combined properties of metals and ceramics, including readily machinability, good thermal and electrical conductivity, high strength and elastic modulus, good oxidation, and corrosion resistance [7, 8]. These properties are attributed to their unique high-order crystalline structures. The M-X octahedral layer and close-packed A-group layer alternatively stack along with the c-direction in the layered hexagonal symmetry structure (group $P6_3/mmc$) of MAX phases. M-X is a strong covalent bonding which is similar to the binary carbide or nitride and displays the ceramic properties, while the M-A is a weaker bond which displays the metallic properties [9–12]. The combined properties suggest the potential applications in elevated-temperature structural devices.

Most of the bulk-form MAX phase has been synthesized through hot-isostatic-pressing (HIP) [13–15] and spark plasma sintering (SPS) [16–18] by sintering a mixed powder of elements or compounds at a very high temperature. MAX-phase thin films have been synthesized by various methods such as magnetron sputtering [19–21], pulsed cathodic arc [22, 23], and chemical vapor deposition [24–27]. High-power impulse magnetron sputtering (HiPIMS), which has programmable pulsed power applying on the cathode, is a promising physical vapor deposition approach for film deposition. It utilizes extremely high current densities in short pulse at lower duty cycle (on-off time ratio <10%) [28]. Zhang et al. reported synthesis of MAX-phase Ti_2AlN films from a

Table 1: The parameters of the HiPIMS and the deposition conditions of the films.

Pulsing parameters	P_a [kW]	P_p [kW]	I_a [A]	V_a [V]	I_d [A/cm^2]
26 Hz 7.0% duty cycle	0.8	24.1	40.0	626.4	0.78
Base pressure					2×10^{-5} torr
Working pressure					5×10^{-3} torr
Substrate temperature					Room temperature
Negative bias voltage					−60 V
Substrate to target distance					12 cm
Deposition time					2 h

(i) P_p and P_a are the power of the peak and average target.
(ii) I_a is the current of the average target in a pulse length.
(iii) V_a is the voltage of the average target.
(iv) I_d is the pulse current density of the peak target.

MAX-phase target by using HiPIMS technique [29]. The films exhibited excellent oxidation and corrosion properties. Field et al. reported the synthesis of MAX-phase Cr_2AlC films by a combinatorial approach, especially comparing the HiPIMS and DC magnetron technique under similar conditions on the Cr target [30]. The HiPIMS coating generally exhibited lower resistivity than the conventional DC magnetron sputtering (DCMS) coating.

Ti_2AlC, as one representative example of Al containing MAX phases, has shown remarkable antioxidation and anticorrosion properties. In particular its film form, as an oxidation and corrosion protective layer, has attracted great attention in recent years. Abdulkadhim et al. got the TiC_x/Al bilayer thin films to investigate the influence of the C content on the products at different annealing temperatures [31]. $x \leq 0.7$ is the appropriate ratio for Al intercalation into the TiC_x to form the MAX phase. Wang et al. obtained the Ti_2AlC thin films through cosputtering of titanium, aluminum, and carbon target at 500°C and then annealing at 800°C and investigated the oxidation behavior of the films [32]. Frodelius et al. obtained the MAX-phase Ti_2AlC through cosputtering the MAX-phase Ti_2AlC and the Ti target, the Ti target was added to balance the excess of the C [33]. More recently, Feng et al. obtained the MAX-phase Ti_2AlC from the $Ti_{50}Al_{50}$ target in Ar/CH_4 atmosphere with CH_4 as the reactive gas at room temperature and annealing at 800°C and investigated the oxidation behaviors of the MAX-phase films [34]. However, the mechanism for the superior oxidation and corrosion properties of MAX-phase Ti_2AlC films still needed to be further investigated. In this study, we synthesized MAX-phase Ti_2AlC films using HiPIMS technique from a MAX-phase Ti_2AlC compound target and postannealing process. The microstructure, oxidation, and corrosion properties of the MAX-phase films were systematically investigated. As a comparison, the oxidation and corrosion measurements of the as-deposited amorphous matrix film were also conducted. And the mechanism for the superior antioxidation and anticorrosion properties of MAX-phase Ti_2AlC thin films was further discussed.

2. Experimental Methods

2.1. Sample Preparation. A MAX-phase Ti_2AlC target (diameter: 80 mm and thickness: 10 mm) was synthesized by spark plasma sintering (SPS) at 1100°C under 30 MPa in vacuum. Electron probe microanalysis (EPMA) showed that the atomic ratio was Ti : Al : C : O = 47.29 : 22.01 : 25.27 : 5.43. X-ray diffraction (XRD) results demonstrated that the Ti_2AlC target was mainly Ti_2AlC MAX phase. Prior to deposition, the polycrystalline Al_2O_3 substrates and stainless steel (SUS304) substrates were ultrasonically cleaned in acetone and alcohol for 20 min. Argon ion bombardment was applied at −800 V bias for 5 min to further clean the substrates. The amorphous matrix Ti-Al-C films were grown at room temperature using a HiPIMS coating system (HIPIMS+ power, Hauzer Techno Coating BV) in the argon (Ar) atmosphere. The film thickness was determined by the deposition time. Table 1 shows the pulsing parameters of the HiPIMS and deposition conditions of the amorphous matrix Ti-Al-C films. The MAX-phase Ti_2AlC films were obtained by annealing the as-deposited amorphous matrix Ti-Al-C films in a tube furnace (DTF-80600-PTFS, Dae Heung Science) at 800°C for 1 h in Ar (99.9999%) atmosphere.

2.2. Film Characterization. The film thickness was measured using a scanning electron microscopy (FE-SEM, Hitachi, S-4800). Electron probe microanalysis was carried out to determine the elementary composition (EPMA, Shimadzu, EPMA-1600). X-ray diffractometer (XRD, D8, ADVANCE Cu Kα, 40 kV, 40 mA) was used to characterize the phase structure of the films. The morphology of the films was investigated by the scanning electron microscope (SEM, Hitachi, S-4800, 15 KV). A high resolution field emission transmission electron microscope (FE-TEM, JEOL, JEM-2100F HR) operated at 200 kV was conducted to further examine the microstructure. The focused ion beam (FIB) technique was used for TEM sample preparation.

2.3. Film Performance. Isothermal oxidation tests for both amorphous matrix Ti-Al-C films and MAX-phase Ti_2AlC films, which were deposited on polycrystalline Al_2O_3

Table 2: The chemistry compositions of the MAX-phase Ti_2AlC target and the films at various temperature.

Composition (atomic %)	Ti	Al	C	O
Target	47.29	22.01	25.27	5.43
As-deposited film	42.73	27.48	24.22	5.57
Film annealed at 800°C	48.02	22.87	23.09	6.02

substrate, were conducted at 800°C in a muffle furnace in static air atmosphere for 1 h to 50 h, respectively. The XRD and TEM analyses were used to analyze the products of the oxidation. The surface and cross section morphology and the thickness of the oxidation layers were observed by SEM and TEM analyses. In order to demonstrate the influence of the oxidation onto the compositions of the films, the SEM-line profiling and the TEM-mapping of energy dispersive X-ray spectrometer (EDX) were also carried out. Thermal-gravimetric analysis (TGA) was carried out by using a TGA instrument (STA409PC, NETZSCH) at temperatures from room temperature to 1300°C in the flowing gas mixture of air and N_2 (air : N_2 = 35 : 15) with an empty pure alumina crucible as an inert reference. The mass gain of the films during heating was then recorded.

The corrosion behaviors of the SUS304 specimens coated with and without films were studied by the potential dynamic polarization (PDP) curves (potentiostat/galvanostat, VersaSTAT 4) in 3.5 wt. % sodium chloride (NaCl) solution at room temperature (RT). The prepared samples, platinum (Pt) mesh, and the saturated calomel electrode (SCE) were used as the working electrode, the counter electrode, and the reference electrode, respectively. The electrode potential range of the measurement was from −1 V to 1 V and the open-circuit corrosion potential was at a scan rate of 1 mV/s.

3. Results and Discussion

3.1. Characterization of the Films

3.1.1. Composition. As shown in Table 2, EPMA measurements were utilized to demonstrate the compositions of the Ti_2AlC target and the Ti-Al-C films. There was a little composition deviation between the films and the target. Compared with the target, the excess of the Al atoms of the as-deposited films should be determined by the longer mean-free-path (λ) compared to the titanium atoms ($\lambda_{Al} > 1.3\lambda_{Ti}$) due to the smaller size of the aluminum atoms [35]. The loss of the Al atoms during annealing at 800°C should be related to the lower vapor pressure of Al. In other MAX phases, for example, the Ga-containing MAX phase, the influence of the vapor pressure also effected the amounts of the Ga atoms [36]. At high temperature, the "A" content was temperature dependent and the evaporation of the "A" element became the dominant factors to influence the compositions of the film. Similar results have also been observed in many MAX-phase studies [8, 20, 37–40]. The incorporation of small amount of oxygen was mainly coming from the impurity of the target fabrication and the film deposition process.

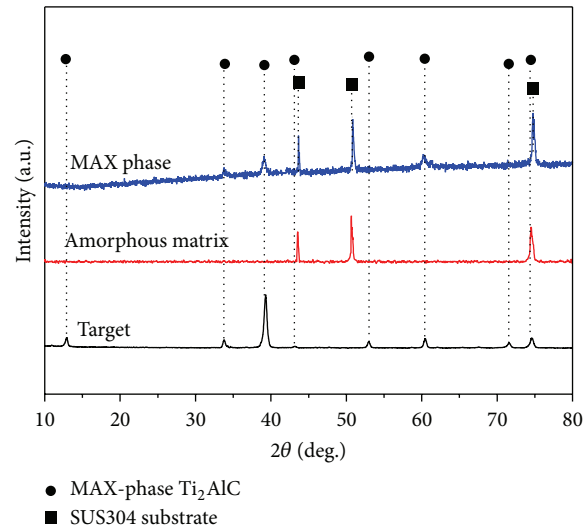

Figure 1: XRD patterns of the MAX-phase Ti_2AlC target, the amorphous matrix film Ti-Al-C, and the MAX-phase Ti_2AlC films on SUS304 substrate.

3.1.2. Structure. Figure 1 shows the XRD analyses of the MAX-phase Ti_2AlC target and as-deposited and annealed Ti-Al-C films on SUS304 substrate, respectively. It was observed that the target was mainly composed of MAX-phase Ti_2AlC. No obvious diffraction peaks in as-deposited films were detected, which indicated that the as-deposited films were amorphous. In contrast, after annealing at 800°C, the amorphous matrix films transformed to polycrystalline MAX-phase films mainly composed of MAX-phase Ti_2AlC, with (100), (103), and (110) planes being identified at 34.02°, 39.55°, and 60.90°, respectively. The transformation at high temperature indicated that high atom activity was required to form the high ordered MAX phase.

Figure 2 shows the SEM images and line-scan EDX analyses of the as-deposited Ti-Al-C and MAX-phase Ti_2AlC films, respectively. As can be found from the cross section (Figures 2(c) and 2(d)), two homogeneous films with a thickness of about 2 μm were formed. Meanwhile, no distinctive crystal was observed from the Ti-Al-C film (Figures 2(a) and 2(b)) indicating that the structure of the Ti-Al-C film was a representative amorphous matrix phase, while a fine and sub-micro equiaxed crystal structure has been observed in the cross section SEM image of the MAX-phase Ti_2AlC (Figures 2(b) and 2(d)). In addition, Figures 2(e) and 2(f) show the line-scan EDX analyses of the amorphous matrix Ti-Al-C film and MAX-phase Ti_2AlC film, respectively.

The characteristic microstructure of the amorphous matrix Ti-Al-C and the MAX-phase Ti_2AlC film is also investigated by high resolution TEM analyses. Figure 3 shows the selected-area electron diffraction (SAED) patterns as well as the HR-TEM images of the amorphous matrix Ti-Al-C and MAX-phase Ti_2AlC film. The SAED pattern and the HR-TEM images shown in Figure 3(b) demonstrated that the structure of the Ti-Al-C film was fine-grained polycrystalline; we defined it as an amorphous matrix phase (the grains are too small to be visible in XRD). Figure 3(d) shows typical

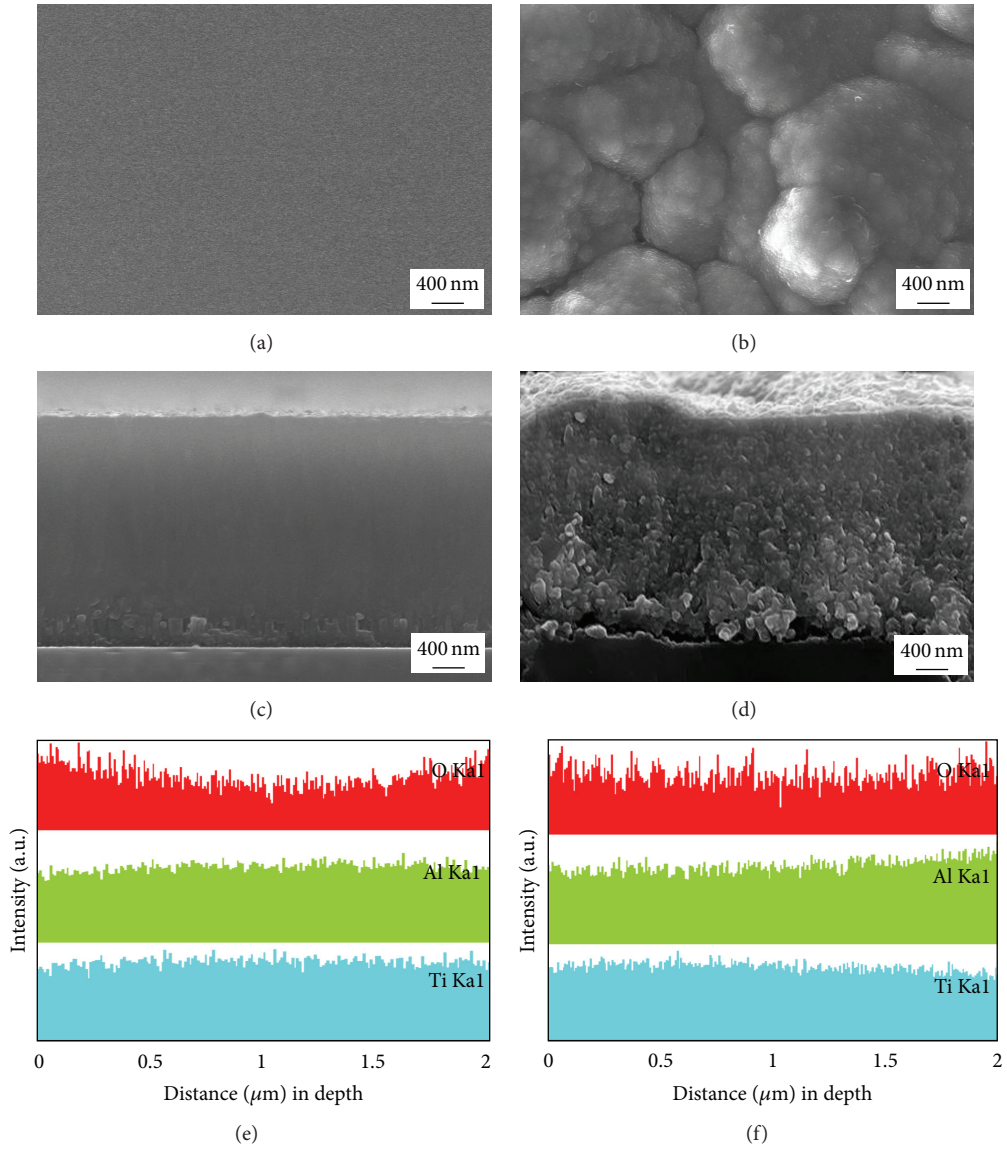

Figure 2: SEM images and line-scan EDX analyses of the (a, c, e) amorphous matrix Ti-Al-C films and (b, d, f) MAX-phase Ti_2AlC films on the Al_2O_3 substrate.

nanolaminated structure of the MAX-phase structure. The SAED pattern of the lattice fringes in the inset also indicated the diffraction patterns of the MAX-phase Ti_2AlC. The characterizations from XRD and TEM results demonstrated that the amorphous matrix Ti-Al-C and MAX-phase Ti_2AlC film were successfully obtained.

3.2. Film Performance

3.2.1. Oxidation Behavior. The isothermal oxidation tests were conducted to investigate oxidation properties of the amorphous matrix Ti-Al-C films and the MAX-phase Ti_2AlC films deposited on polycrystalline Al_2O_3 substrates. Figure 4 exhibits the XRD analyses of the films through isothermal oxidation at 800°C for 5 h. Alumina was considered to be formed on both amorphous matrix and MAX-phase films during oxidation; however, the formed Al_2O_3 could not be identified due to the relatively strong peak intensity of the Al_2O_3 substrates, while the peaks corresponding to TiO_2 were easily detected. In Figure 4(a), the relatively strong peaks of the TiO_2 emerged after oxidation, which indicated the serious attack of the oxygen on the surface of the amorphous matrix Ti-Al-C film. In Figure 4(b), after oxidation for 5 h, MAX-phase Ti_2AlC was still the dominant phase in the film with no obvious TiO_2 peak being detected, which meant the MAX-phase Ti_2AlC showed better oxidation resistance.

The true structure of the oxidation region of the MAX-phase Ti_2AlC film during the oxidation was further investigated by the HR-TEM, the SAED pattern, and the point EDX scan as illustrated in Figure 5. The polycrystalline structure of the oxide layer was clearly revealed by the combination SAED pattern with the point EDX analysis. Electron diffraction

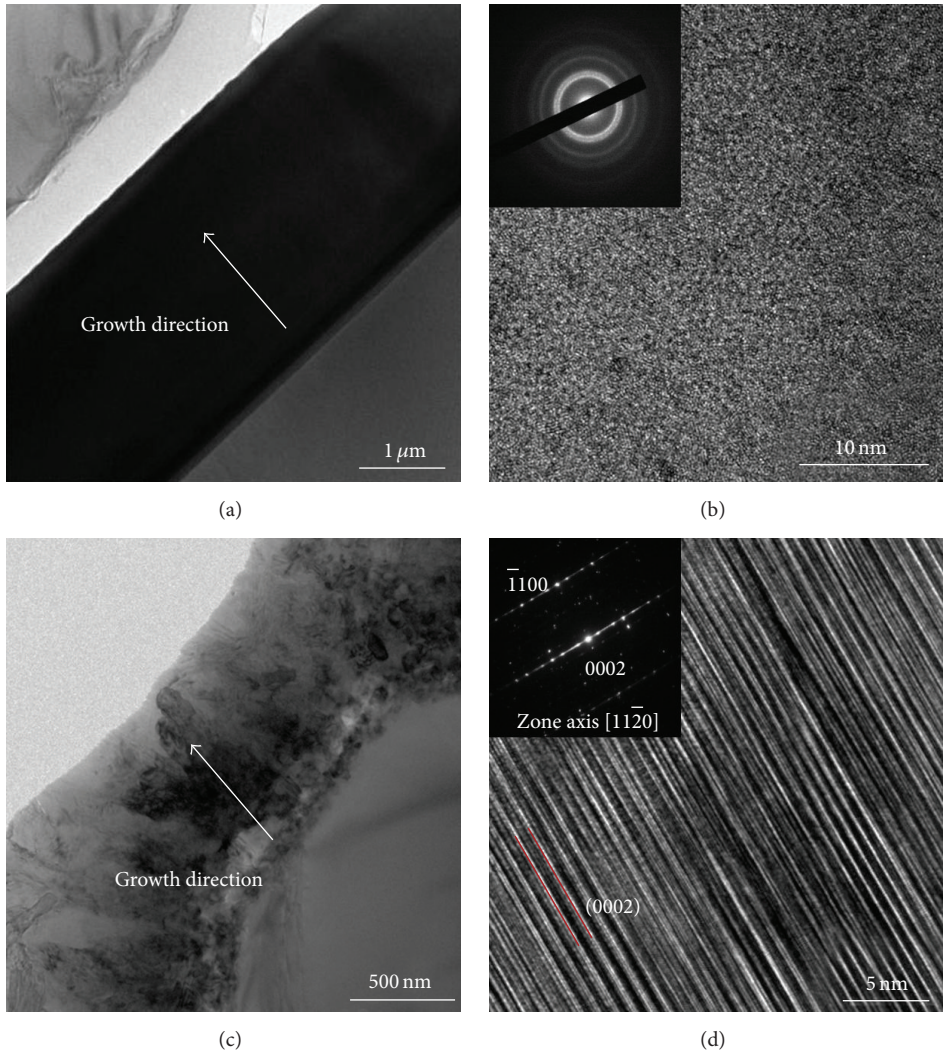

Figure 3: (a) Cross section TEM image of the amorphous matrix Ti-Al-C films, (b) high resolution TEM image from the region marked with red square and insets showing the SAED of the amorphous matrix Ti-Al-C films, (c) cross section TEM image of the MAX-phase Ti_2AlC films, and (d) high resolution TEM image from the region marked with red square insets showing the SAED along the [11$\bar{2}$0] zone axis of the MAX-phase Ti_2AlC films.

region was oriented along the [$\bar{1}$11] zone axis. The oxide layer was confirmed to have a hexagonal aluminium oxide with a formula $(Al_2O_3)_{5.333}$ (cubic, space group *Fd-3m*, ICSD ID: 11569) [41]. EDX point scan indicates that the chemistry composition of the cross point is 37.43% Al, 62.43% O, and Ti 0.14% in atomic ratio as shown in Figure 5(c).

Figure 6 shows the surface and cross-sectional SEM morphologies and line-scan EDX analyses of the films on Al_2O_3 substrates after isothermal oxidation at 800°C for 5 h, respectively. An oxide layer was formed on the surface of both films. The oxide layer on the amorphous matrix Ti-Al-C film exhibited loose morphology full of cracks, which could not prevent the attack of oxygen into the film. It was further proved by the cross-sectional SEM morphologies and its line-scan EDX analysis that oxygen existed throughout the depth of amorphous matrix film after the oxidation, while a continuous and homogenous oxide layer with dense microstructure was formed on the MAX-phase Ti_2AlC film. Also the line-scan EDX analysis shows that the oxide layer was Al-rich and the oxygen signal below the oxide layer was significantly lower than that of the amorphous matrix Ti-Al-C after oxidation, which indicated that the dense oxide layer acted as a good barrier for oxygen diffusion into the MAX-phase films during oxidation.

TEM test and EDX mapping were also performed on the oxide layer to explore the structure of the films. Figure 7 exhibits the microstructure and EDX mapping of the Al, Ti, and O atoms after isothermal oxidation at 800°C for 5 h on polycrystalline Al_2O_3 substrate from the amorphous matrix Ti-Al-C films (Figure 7(a)) and the MAX-phase Ti_2AlC film (Figure 7(e)). Results clearly confirmed that the morphology of the amorphous matrix Ti-Al-C film and the MAX-phase Ti_2AlC film after oxidation agrees well with the SEM images in Figure 6. More importantly, the EDX mapping in

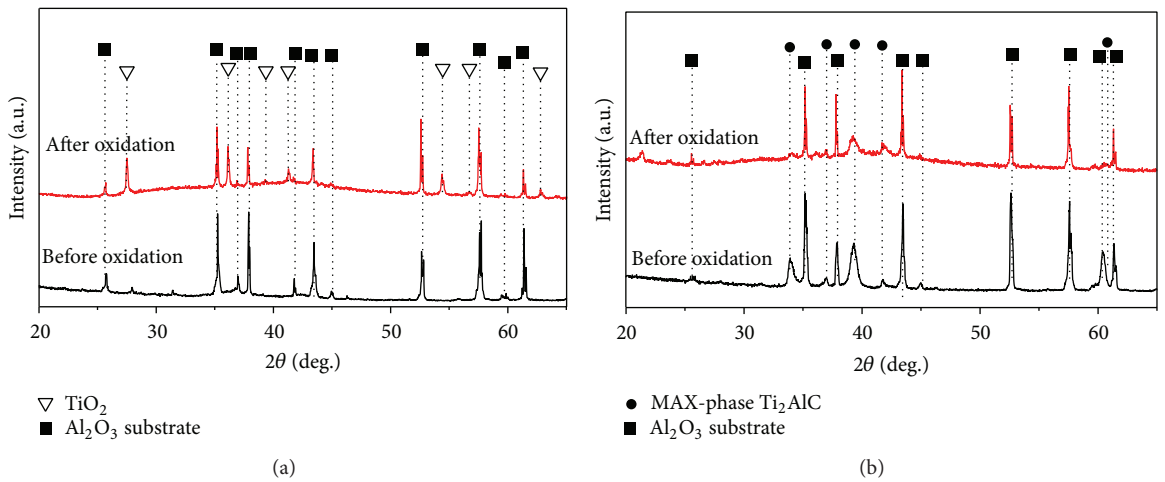

FIGURE 4: XRD analyses of the films before and after isothermal oxidation at 800°C for 5 h: (a) amorphous matrix Ti-Al-C films and (b) MAX-phase Ti_2AlC films on polycrystalline Al_2O_3 substrate.

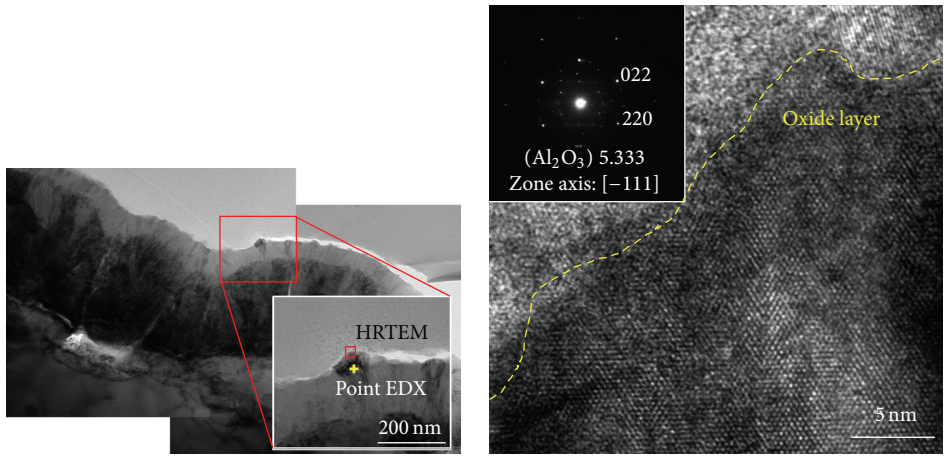

Element	Mass (%)	Atom (%)
O	49.56	62.43
Al	50.12	37.43
Ti	0.33	0.14

(c)

FIGURE 5: (a) Cross section TEM image of the MAX-phase Ti_2AlC films after isothermal oxidation at 800°C for 5 h polycrystalline Al_2O_3 substrate, (b) high resolution TEM image from the region marked with red square insets showing the SAED along the $[\bar{1}11]$ zone axis, and (c) the point EDX of the yellow cross point of the oxide layer.

Figures 7(b)–7(d) indicates the even distributions of the Al and Ti atoms, suggesting a simultaneous oxidation of the Al and Ti (the formation of the Al-Ti-O compound) on the amorphous matrix Ti-Al-C film, while, in Figures 7(f)–7(h), there was a Al-rich region on the top of the film, indicating the preferred and rapid Al atoms migration of the MAX-phase Ti_2AlC film.

To further characterize the oxidation behavior of the MAX-phase Ti_2AlC films, the time-dependent oxidation test at 800°C was performed. Figure 8 shows the XRD diffraction patterns of the MAX-phase Ti_2AlC films after oxidation for 1, 3, 5, 10, 20, 30, and 50 h at 800°C, respectively. It was observed that no peaks corresponding to TiO_2 were detected before 20 h, which indicated that the dense Al_2O_3 layer formed on the film surface performed good protection against oxidation diffusion before 20 h. And further increase of oxidation time to 50 h led to significant increase of intensity of the TiO_2. Figure 9 shows the surface and cross-sectional SEM

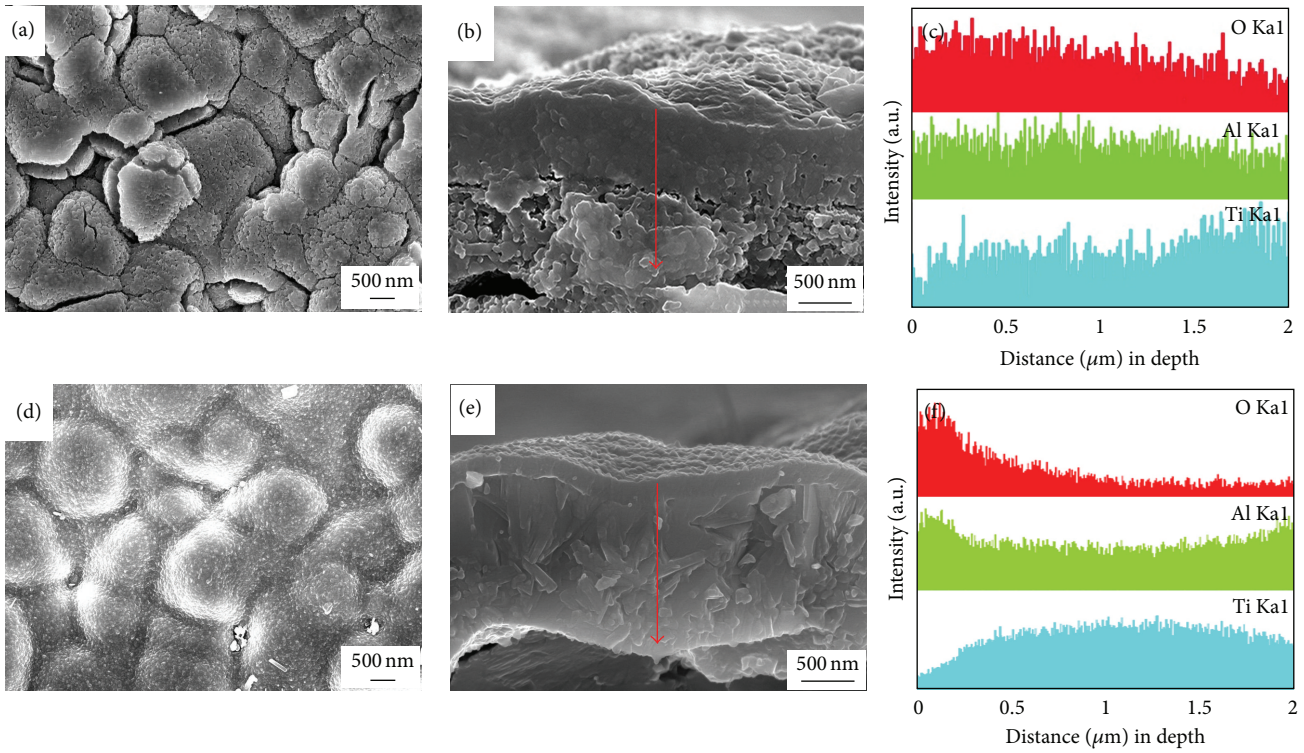

FIGURE 6: SEM images and line-scan EDX analyses of the films after isothermal oxidation: (a, b, c) amorphous matrix Ti-Al-C films at 800°C for 5 h and (d, e, f) MAX-phase Ti_2AlC film at 800°C for 5 h on polycrystalline Al_2O_3 substrate.

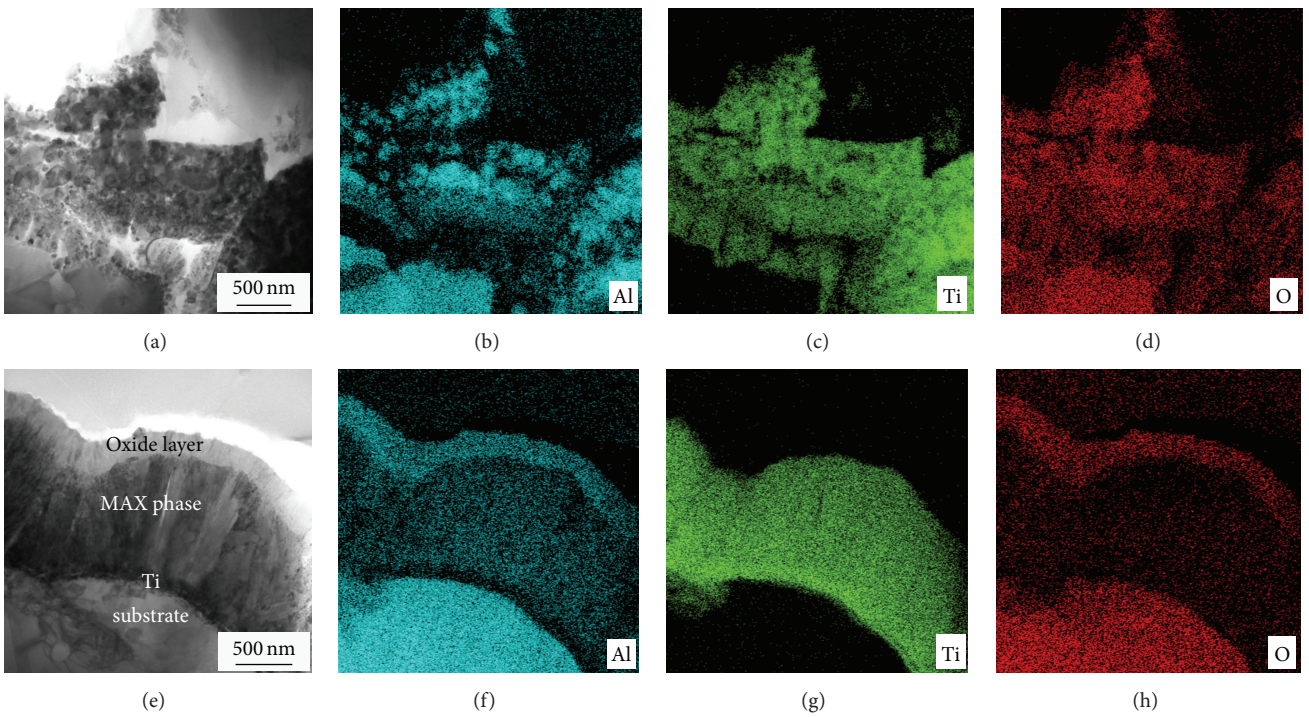

FIGURE 7: Microstructure and chemistry of the films after isothermal oxidation. (a) Low magnification TEM image of amorphous matrix Ti-Al-C films at 800°C for 5 h polycrystalline Al_2O_3 substrate. The EDX mapping of the (b) Al, (c) Ti, and (d) O. (e) Low magnification TEM image of MAX-phase Ti_2AlC film at 800°C for 5 h on polycrystalline Al_2O_3 substrate. The EDX mapping of the (f) Al, (g) Ti, and (h) O.

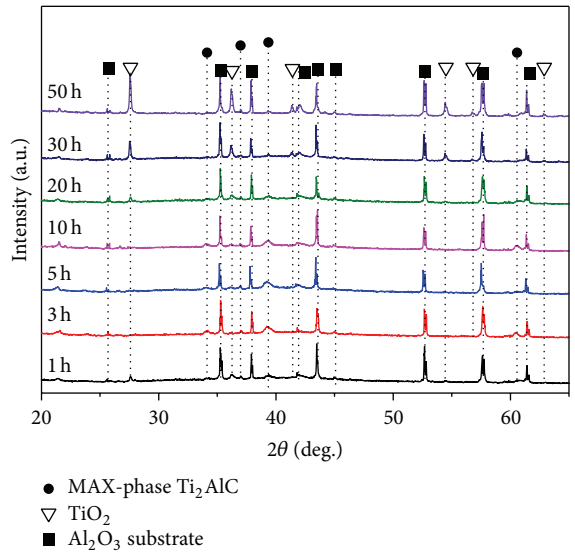

FIGURE 8: X-ray diffraction patterns of MAX-phase Ti_2AlC films after oxidation at 800°C at various time on polycrystalline Al_2O_3 substrate.

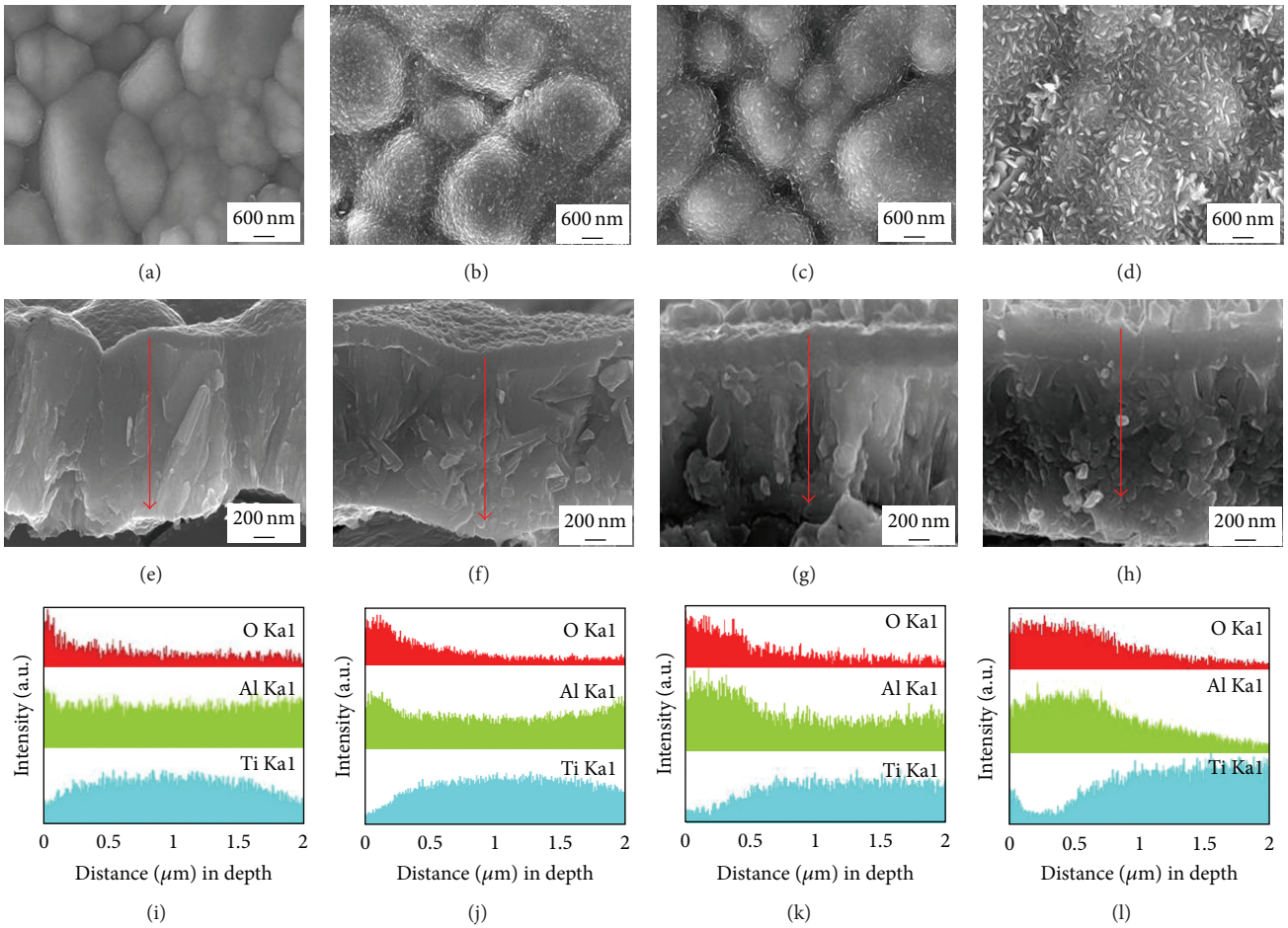

FIGURE 9: SEM images and line-scan EDX analyses of the MAX-phase Ti_2AlC films after isothermal oxidation at 800°C at various time on polycrystalline Al_2O_3 substrate: (a, e, i) 1 h, (b, f, j) 5 h, (c, g, k) 30 h, and (d, h, l) 50 h.

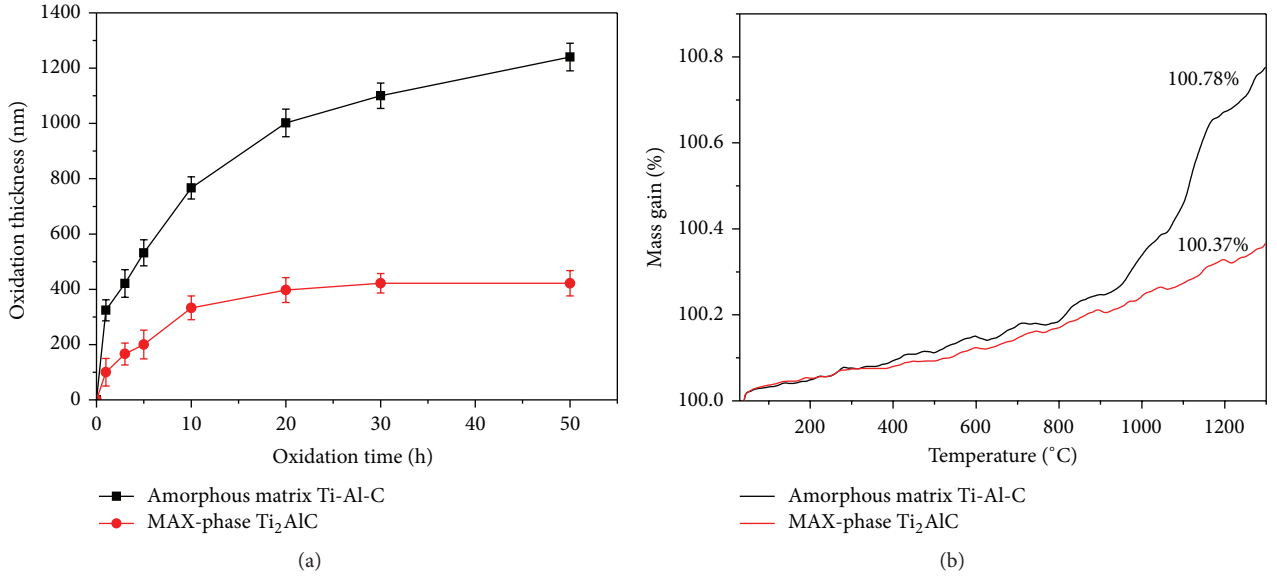

FIGURE 10: (a) The thickness of the oxide layers formed on amorphous matrix Ti-Al-C and MAX-phase Ti_2AlC films after oxidation at 800°C as a function of oxidation time and (b) TGA analyses of the amorphous matrix Ti-Al-C and MAX-phase Ti_2AlC films after the oxidation from RT to 1300°C at 15 K/min heating rate in the flowing $Ar : N_2 = 35 : 15$ atmosphere on polycrystalline Al_2O_3 substrate.

morphologies and the line-scan EDX analysis of the films on Al_2O_3 substrates after isothermal oxidation at 800°C at various times. For the sample after oxidation for 1 h, no oxide layer was observed. As the oxidation time increases to 30 h, obvious increase of the dense oxide layer could be seen, which was mainly composed of Al_2O_3. After the MAX-phase film oxidized for over 50 h, the surface of the film became much rougher and needle-like crystals appeared which represented the TiO_2 starting to form on the film surface, while the film below the oxide layer remained being well protected. This result is in good agreement with the XRD data in Figure 8.

Figure 10 shows the thickness increase of the oxide layer formed on film surface and the mass gain of the amorphous matrix Ti-Al-C and MAX-phase Ti_2AlC films as a function of the oxidation time and oxidation temperature, respectively. As seen in Figure 10(a), the amorphous matrix Ti-Al-C films exhibited oxidation behavior following the parabolic oxidation law while the MAX-phase Ti_2AlC films followed the logarithmic oxidation law due to the phase structure difference. The TGA test was carried out to investigate the oxidation temperature effect on the amorphous matrix Ti-Al-C films and MAX-phase Ti_2AlC films and to seek their failure point (the temperature where the film lost protective function) against oxidation. As shown in Figure 10(b), a greater mass gain rate was observed for the Ti-Al-C amorphous matrix films, as compared with MAX-phase film, and it exhibited a significant increase at temperature at about 800°C, which meant the failure point for the amorphous matrix Ti-Al-C film was 800°C, while the MAX-phase Ti_2AlC films exhibited a continuous increase of mass gain, with no obvious changing point that could be found. In this study, the thickness of the MAX-phase Ti_2AlC film was only 2 μm. The amount of the Al was limited. Correspondingly, in bulk-form MAX phase, the Al atoms are very sufficient, so the protection of the Al is much more significant than the film form [42–44]. Thus, thicker MAX-phase film is preferred for oxidation resistance.

TABLE 3: Corrosion analyses from potential dynamic polarization curves in the 3.5 wt.% NaCl aqueous solution.

	SUS304 substrate	Amorphous matrix Ti-Al-C	MAX-phase Ti_2AlC
I_{corr} (A/cm^2)	1.91×10^{-5}	1.44×10^{-6}	5.82×10^{-8}
E_{corr} (V vs. SCE)	−0.529	−0.618	−0.301

Because of the special nanolaminated microstructure of the MAX-phase Ti_2AlC, the metallic-like Ti-Al bonds are relatively weaker than the covalent Ti-C bonds; the aluminum atoms have higher activity and higher migration rate than the titanium atoms. Therefore, at the initial stage of the oxidation, the aluminum atoms can migrate out to form a relatively high density Al_2O_3 layer, which can prohibit the attack of oxygen atoms to the inward of the films. So it provided a more effective protection to the substrate. For the amorphous matrix Ti-Al-C film, the activity of aluminum atoms is lower. The oxidized surface of the film is a mixture of the Al_2O_3 and TiO_2 which are much loose and porous; the attack of oxygen into the film proceeds with no effective obstacles, which means it cannot be a helpful protection against the attack of the oxygen compared with the pure and high density Al_2O_3 layer.

3.2.2. Corrosion Behavior. Figure 11 shows the polarization curves of the bare SUS304 substrate, MAX-phase Ti_2AlC, and the amorphous matrix Ti-Al-C coated samples in 3.5 wt. % NaCl aqueous solution, respectively. The corrosion current density (I_{corr}), calculated by using Tafel equation [45], and corrosion potentials (E_{corr}) were listed in Table 3.

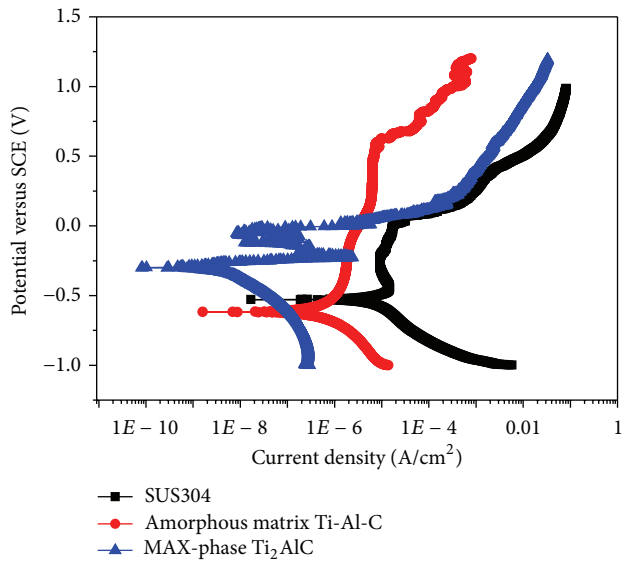

FIGURE 11: The potentiodynamic polarization curves of the amorphous matrix Ti-Al-C, MAX-phase Ti_2AlC films, and the SUS304 substrate in the 3.5 wt. % NaCl aqueous solution.

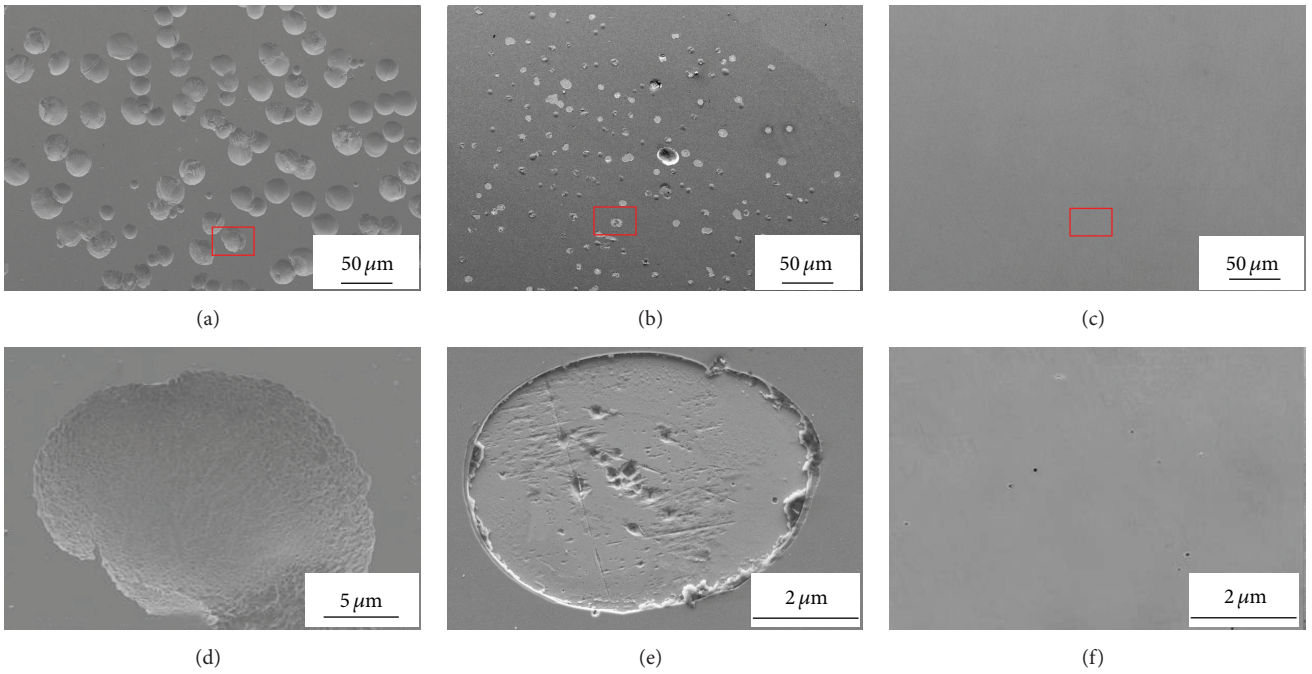

FIGURE 12: SEM images of the (a, d) SUS304 substrate, (b, e) amorphous matrix Ti-Al-C, and (c, f) MAX-phase Ti_2AlC films after corrosion test in the 3.5 wt. % NaCl aqueous solution.

I_{corr} significantly decreased after by applying films, which revealed that the substrate was effectively protected from the corrosive media. Compared with the sample coated by amorphous matrix Ti-Al-C, the MAX-phase Ti_2AlC coated sample exhibits lower I_{corr} of 5.82×10^{-8} A/cm^2 and higher E_{corr} of −0.301 V, indicating better corrosion resistance and protective efficiency.

Figure 12 shows the surface SEM images of the MAX-phase Ti_2AlC, the amorphous matrix Ti-Al-C deposited on the SUS304, and bare SUS304 substrate after the corrosion behavior in 3.5 wt. % NaCl aqueous solution. Obvious corrosive failure, with totally open pits over all the film, could be observed on the surface of bare SUS304 substrate and amorphous matrix Ti-Al-C deposited sample (Figures 12(a)–12(d)). However, no obvious pitting damage and pores were observed on the surface of the MAX-phase Ti_2AlC coated sample (Figures 12(e) and 12(f)), which indicated that it suffered much less corrosion attack and

performed the best corrosion resistance during the corrosion process. It was considered that the high active Al atoms could readily migrate out to the surface of the film to form a high density Al_2O_3 oxide layer, which passivated the surface and prevented further corrosion behavior during the chemical attack due to the special atomic arrangement of the MAX phase, in which Al-C bonds were relatively weaker. Thus, the MAX-phase Ti_2AlC film provided a more effective protection compared with the amorphous matrix Ti-Al-C film.

4. Conclusion

In this study, nanolaminated MAX-phase Ti_2AlC thin films were fabricated by high-power impulse magnetron sputtering (HiPIMS) from a Ti_2AlC MAX-phase target. The amorphous matrix Ti-Al-C films were deposited at room temperature, while the MAX-phase Ti_2AlC films were obtained through annealing process of the as-deposited amorphous films. The microstructure, oxidation resistance, and corrosion resistance of the amorphous matrix Ti-Al-C and MAX-phase Ti_2AlC films were comparatively investigated. The MAX-phase Ti_2AlC films exhibited less mass gain rate and thinner thickness of the oxide layer compared with the amorphous matrix Ti-Al-C film. And the amorphous matrix Ti-Al-C films exhibited oxidation behavior following the parabolic oxidation law, while the MAX-phase Ti_2AlC films followed the logarithmic oxidation law. Meanwhile the MAX-phase Ti_2AlC films showed higher corrosion potential value (E_{corr}) and lower corrosion current density value (I_{corr}) compared with the amorphous films, which indicated better corrosion resistance. The mechanism for superior antioxidation and anticorrosion properties of MAX-phase films was related to a quick formation of stable and high density of Al_2O_3 layer on the films due to fast outmigration of aluminum atoms, which acted as a good barrier layer for oxygen diffusion to prevent further oxidation.

Conflict of Interests

The authors declare that there is no conflict of interests regarding the publication of this paper.

Acknowledgment

This study was supported by Global Frontier Program through the Global Frontier Hybrid Interface Materials (GFHIM) of the National Research Foundation of Korea (NRF) funded by the Ministry of Science, ICT & Future Planning (2013M3A6B1078874).

References

[1] M. W. Barsoum, "The $M_{n+1}AX_n$ phases: a new class of solids: thermodynamically stable nanolaminates," *Progress in Solid State Chemistry*, vol. 28, no. 1, pp. 201–281, 2000.

[2] P. Eklund, M. Beckers, U. Jansson, H. Högberg, and L. Hultman, "The $M_{n-1}AX_n$ phases: materials science and thin-film processing," *Thin Solid Films*, vol. 518, no. 8, pp. 1851–1878, 2010.

[3] J. Wang and Y. Zhou, "Recent progress in theoretical prediction, preparation, and characterization of layered ternary transition-metal carbides," *Annual Review of Materials Research*, vol. 39, pp. 415–443, 2009.

[4] M. W. Barsoum, D. Brodkin, and T. El-Raghy, "Layered machinable ceramics for high temperature applications," *Scripta Materialia*, vol. 36, no. 5, pp. 535–541, 1997.

[5] W. Jeitschko and H. Nowotny, "Die Kristallstruktur von Ti_3SiC_2-ein neuer Komplexcarbid-Typ," *Monatshefte für Chemie und verwandte Teile anderer Wissenschaften*, vol. 98, no. 2, pp. 329–337, 1967.

[6] V. H. Nowotny, "Strukturchemie einiger verbindungen der übergangsmetalle mit den elementen C, Si, Ge, Sn," *Progress in Solid State Chemistry*, vol. 5, pp. 27–70, 1971.

[7] P. O. Å. Persson, S. Kodambaka, I. Petrov, and L. Hultman, "Epitaxial Ti_2AlN(0 0 0 1) thin film deposition by dual-target reactive magnetron sputtering," *Acta Materialia*, vol. 55, no. 13, pp. 4401–4407, 2007.

[8] J. Alami, P. Eklund, J. Emmerlich et al., "High-power impulse magnetron sputtering of Ti-Si-C thin films from a Ti_3SiC_2 compound target," *Thin Solid Films*, vol. 515, no. 4, pp. 1731–1736, 2006.

[9] J. Wang and Y. Zhou, "Dependence of elastic stiffness on electronic band structure of nanolaminate M_2A1C (M=Ti,V,Nb, and Cr) ceramics," *Physical Review B*, vol. 69, no. 21, Article ID 214111, 2004.

[10] Z. Sun, R. Ahuia, S. Li, and J. M. Schneider, "Structure and bulk modulus of M_2 AIC (M=Ti, V, and Cr)," *Applied Physics Letters*, vol. 83, no. 5, pp. 899–901, 2003.

[11] Y. Zhou and Z. Sun, "Electronic structure and bonding properties in layered ternary carbide Ti_3SiC_2," *Journal of Physics Condensed Matter*, vol. 12, no. 28, p. L457, 2000.

[12] J. Wang, J. Wang, A. Li, J. Li, and Y. Zhou, "Theoretical study on the mechanism of anisotropic thermal properties of Ti_2AlC and Cr_2AlC," *Journal of the American Ceramic Society*, vol. 97, no. 4, pp. 1202–1208, 2014.

[13] W. Yu, V. Mauchamp, T. Cabioc'h et al., "Solid solution effects in the $Ti_2Al(C_xN_y)$ MAX phases: synthesis, microstructure, electronic structure and transport properties," *Acta Materialia*, vol. 80, pp. 421–434, 2014.

[14] N. V. Tzenov and M. W. Barsoum, "Synthesis and characterization of Ti_3AlC_2," *Journal of the American Ceramic Society*, vol. 83, no. 4, pp. 825–832, 2000.

[15] M. W. Barsoum, "A progress report on Ti_3SiC_2, Ti_3GeC_2, and the H-phases, M_2BX," *Journal of Materials Synthesis and Processing*, vol. 5, no. 3, pp. 197–216, 1997.

[16] E.-S. Choi, J. Sung, Q.-M. Wang, K.-H. Kim, A. Busnaina, and M. C. Kang, "Material properties and machining performance of hybrid Ti_2AlN bulk material for micro electrical discharge machining," *Transactions of Nonferrous Metals Society of China*, vol. 22, no. 3, pp. s781–s786, 2012.

[17] Z. F. Zhang, Z. M. Sun, H. Hashimoto, and T. Abe, "Application of pulse discharge sintering (PDS) technique to rapid synthesis of Ti_3SiC_2 from Ti/Si/C powders," *Journal of the European Ceramic Society*, vol. 22, no. 16, pp. 2957–2961, 2002.

[18] Z.-F. Zhang, Z. M. Sun, H. Hashimoto, and T. Abe, "Fabrication and microstructure characterization of Ti_3SiC_2 synthesized from Ti/Si/2TiC powders using the pulse discharge sintering (PDS) technique," *Journal of the American Ceramic Society*, vol. 86, no. 3, pp. 431–436, 2003.

[19] D. P. Sigumonrong, J. Zhang, Y. Zhou, D. Music, and J. M. Schneider, "Synthesis and elastic properties of V_2AlC thin films by magnetron sputtering from elemental targets," *Journal of Physics D: Applied Physics*, vol. 42, no. 18, Article ID 185408, 2009.

[20] O. Wilhelmsson, P. Eklund, H. Högberg, L. Hultman, and U. Jansson, "Structural, electrical and mechanical characterization of magnetron-sputtered V-Ge-C thin films," *Acta Materialia*, vol. 56, no. 11, pp. 2563–2569, 2008.

[21] J. M. Schneider, D. P. Sigumonrong, D. Music et al., "Elastic properties of Cr_2AlC thin films probed by nanoindentation and ab initio molecular dynamics," *Scripta Materialia*, vol. 57, no. 12, pp. 1137–1140, 2007.

[22] M. C. Guenette, M. D. Tucker, M. Ionescu, M. M. M. Bilek, and D. R. McKenzie, "Cathodic arc co-deposition of highly oriented hexagonal Ti and Ti_2AlC MAX phase thin films," *Thin Solid Films*, vol. 519, no. 2, pp. 766–769, 2010.

[23] J. Rośn, L. Ryves, P. O. Å. Persson, and M. M. M. Bilek, "Deposition of epitaxial Ti_2AlC thin films by pulsed cathodic arc," *Journal of Applied Physics*, vol. 101, no. 5, Article ID 056101, 2007.

[24] J. J. Nickl, K. K. Schweitzer, and P. Luxenberg, "Gasphasenabscheidung im system Ti–Si–C," *Journal of the Less-Common Metals*, vol. 26, no. 3, pp. 335–353, 1972.

[25] H. Fakih, S. Jacques, M.-P. Berthet, F. Bosselet, O. Dezellus, and J.-C. Viala, "The growth of Ti_3SiC_2 coatings onto SiC by reactive chemical vapor deposition using H_2 and $TiCl_4$," *Surface and Coatings Technology*, vol. 201, no. 6, pp. 3748–3755, 2006.

[26] H. Fakih, S. Jacques, O. Dezellus, M. P. Berthet, F. Bosselet, and J. C. Sacerdote-Peronnet, "Phase equilibria and reactive chemical vapor deposition (RCVD) of Ti_3SiC_2," *Journal of Phase Equilibria and Diffusion*, vol. 29, no. 3, pp. 239–246, 2008.

[27] S. Hassani, J.-E. Klemberg-Sapieha, and L. Martinu, "Mechanical, tribological and erosion behaviour of super-elastic hard Ti–Si–C coatings prepared by PECVD," *Surface and Coatings Technology*, vol. 205, no. 5, pp. 1426–1430, 2010.

[28] J. Alami, S. Bolz, and K. Sarakinos, "High power pulsed magnetron sputtering: fundamentals and applications," *Journal of Alloys and Compounds*, vol. 483, no. 1-2, pp. 530–534, 2009.

[29] T. F. Zhang, Q. M. Wang, J. Lee, P. Ke, R. Nowak, and K. H. Kim, "Nanocrystalline thin films synthesized from a Ti_2AlN compound target by high power impulse magnetron sputtering technique," *Surface and Coatings Technology*, vol. 212, pp. 199–206, 2012.

[30] M. R. Field, P. Carlsson, P. Eklund et al., "A combinatorial comparison of DC and high power impulse magnetron sputtered Cr_2AlC," *Surface and Coatings Technology*, vol. 259, pp. 746–750, 2014.

[31] A. Abdulkadhim, T. Takahashi, D. Music, F. Munnik, and J. M. Schneider, "MAX phase formation by intercalation upon annealing of TiC_x/Al ($0.4 \leq x \leq 1$) bilayer thin films," *Acta Materialia*, vol. 59, no. 15, pp. 6168–6175, 2011.

[32] Q. M. Wang, W. Garkas, A. F. Renteria, C. Leyens, H. W. Lee, and K. H. Kim, "Oxidation behaviour of Ti-Al-C films composed mainly of a Ti_2AlC phase," *Corrosion Science*, vol. 53, no. 9, pp. 2948–2955, 2011.

[33] J. Frodelius, P. Eklund, M. Beckers, P. O. Å. Persson, H. Högberg, and L. Hultman, "Sputter deposition from a Ti_2AlC target: process characterization and conditions for growth of Ti_2AlC," *Thin Solid Films*, vol. 518, no. 6, pp. 1621–1626, 2010.

[34] Z. Feng, P. Ke, Q. Huang, and A. Wang, "The scaling behavior and mechanism of Ti_2AlC MAX phase coatings in air and pure water vapor," *Surface and Coatings Technology*, vol. 272, pp. 380–386, 2015.

[35] P. O. Å. Persson, C. Höglund, J. Birch, and L. Hultman, "$Ti_2Al(O,N)$ formation by solid-state reaction between substoichiometric TiN thin films and Al_2O_3 (0001) substrates," *Thin Solid Films*, vol. 519, no. 8, pp. 2421–2425, 2011.

[36] C. Hu, C.-C. Lai, Q. Tao et al., "Mo_2Ga_2C: a new ternary nanolaminated carbide," *Chemical Communications*, vol. 51, no. 30, pp. 6560–6563, 2015.

[37] C. Walter, D. P. Sigumonrong, T. El-Raghy, and J. M. Schneider, "Towards large area deposition of Cr_2AlC on steel," *Thin Solid Films*, vol. 515, no. 2, pp. 389–393, 2006.

[38] A. Abdulkadhim, M. T. Baben, T. Takahashi et al., "Crystallization kinetics of amorphous Cr_2AlC thin films," *Surface and Coatings Technology*, vol. 206, no. 4, pp. 599–603, 2011.

[39] P. Eklund, M. Beckers, J. Frodelius, H. Högberg, and L. Hultman, "Magnetron sputtering of Ti_3SiC_2 thin films from a Ti_3SiC_2 compound target," *Journal of Vacuum Science & Technology A: Vacuum, Surfaces, and Films*, vol. 25, no. 5, pp. 1381–1388, 2007.

[40] J. Emmerlich, D. Music, P. Eklund et al., "Thermal stability of Ti_3SiC_2 thin films," *Acta Materialia*, vol. 55, no. 4, pp. 1479–1488, 2007.

[41] K. Shirasuka, H. Yanagida, G. Yamaguchi, and Y. Kyokaishi, "The preparation of eta alumina and its structure," *Journal of the Ceramic Assocation*, vol. 84, pp. 610–613, 1976.

[42] D. J. Tallman, B. Anasori, and M. W. Barsoum, "A critical review of the oxidation of Ti_2AlC, Ti_3AlC_2 and Cr_2AlC in air," *Materials Research Letters*, vol. 1, no. 3, pp. 115–125, 2013.

[43] D. Horlait, S. Grasso, N. Al Nasiri, P. A. Burr, and W. E. Lee, "Synthesis and oxidation testing of MAX phase composites in the Cr–Ti–Al–C quaternary system," *Journal of the American Ceramic Society*, 2015.

[44] J. L. Smialek, "Kinetic aspects of Ti_2AlC MAX phase oxidation," *Oxidation of Metals*, vol. 83, pp. 351–366, 2015.

[45] G. Rocchini, "The determination of tafel slopes by the successive approximation method," *Corrosion Science*, vol. 37, no. 6, pp. 987–1003, 1995.